

# Chiral Majorana Hinge Modes in Superconducting Dirac Materials

Bo Fu,<sup>1</sup> Zi-Ang Hu,<sup>1</sup> Chang-An Li,<sup>2</sup> Jian Li,<sup>3,4</sup> and Shun-Qing Shen<sup>1,\*</sup>

<sup>1</sup>*Department of Physics, The University of Hong Kong, Pokfulam Road, Hong Kong, China*

<sup>2</sup>*Institute for Theoretical Physics and Astrophysics,*

*University of Wurzburg, D-97074 Wurzburg, Germany*

<sup>3</sup>*School of Science, Westlake University, 18 Shilongshan Road, Hangzhou 310024, Zhejiang Province, China*

<sup>4</sup>*Institute of Natural Sciences, Westlake Institute for Advanced Study,*

*18 Shilongshan Road, Hangzhou 310024, Zhejiang Province, China*

(Dated: October 30, 2020)

Chiral Majorana hinge modes are characteristic of a second-order topological superconductor in three dimensions. Here we systematically study pairing symmetry in the point group  $D_{2h}$ , and find that the leading pairing channels can be of  $s$ -,  $d$ -, and  $s + id$ -wave pairing in Dirac materials. Except for the odd-parity  $s$ -wave pairing superconductivity, the  $s + id$ -wave pairing superconductor is topologically nontrivial and possesses Majorana hinge and surface modes. The chiral Majorana hinge modes can be characterized by a winding number of the quadrupole moment, or quantized quadrupole moment at the symmetrically invariant point. Our findings suggest the strong spin-orbital coupling, crystalline symmetries and electron-electron interaction in the Dirac materials may provide a microscopic mechanism to realize chiral Majorana hinge modes without utilizing the proximity effect or external fields.

*Introduction* Majorana modes are the quasiparticles around a topological superconductor, and may have the potential application in topological quantum computations [1–6]. Over the last two decades intensive efforts have been made to realize topological superconductors [7–14]. The Majorana edge modes in a  $p_x + ip_y$  spinless superconductor, a superconducting analog of quantum Hall effect state, move in a dissipationless and unidirectional way, i.e., are chiral, because of violation of time-reversal symmetry [15–18]. As the  $p$ -wave superconductor is rare in nature, a hybrid system of quantum anomalous Hall insulator and superconductor was alternatively proposed to realize the chiral topological superconductor [19–21]. However the existence of chiral Majorana modes are still inconclusive [22–26], although several schemes for detection and application are proposed [27–29]. Those proposals often rely heavily on the proximity effect or need an external magnetic field to break the time reversal symmetry, which all make them difficult to be realized in experiments. Very recently, a significant advance in the research of topological quantum phases is a generalization to higher order topological insulators and superconductors that can host localized modes near the corner, hinge or vertex of a system [30–45]. Several theoretical proposals have been put forward to realize the Majorana corner modes in second-order topological superconductors [46–65]. In three dimensions, chiral Dirac modes can emerge along a hinge between two surface planes on which the two gapped surface modes encounter when the time-reversal symmetry is broken [66–69]. This opens a new avenue to search chiral Majorana modes in topological materials.

Here we investigate all possible superconducting pairing channels in three-dimensional (3D) massive Dirac materials with the  $D_{2h}$  point group symmetry at the mean-field level with long-ranged interactions. We find that

the leading pairing channel can be  $s$ -,  $d$ - or  $s + id$ -wave pairing by varying the relative strength of the intra- and inter-orbital interactions. The  $s$ -wave pairing is topologically nontrivial under time-reversal invariance and possesses gapless Majorana surface mode as proposed by Fu and Berg [70] and Sato [71]. For the  $s + id$ -wave pairing channel, inclusion of  $d_{xy}$ -wave pairing breaks the time-reversal symmetry and inversion symmetry, but preserves the combination of these two symmetries. Consequently, the system becomes a second-order topological superconductor with chiral Majorana hinge modes circulating along the four hinges parallel to the  $z$ -axis. The topology behind chiral Majorana hinge modes can be characterized by a winding number of the quadrupole moment, or the quantized quadrupole moment at the particle-hole invariant momentum. This establishes a robust and new bulk-boundary correspondence for the topological states of matter.

*Model* We investigate possible pairing channels in 3D Dirac materials with  $D_{2h}$  point group symmetry and time reversal symmetry by utilizing the symmetry analysis in the irreducible representations of the group. The normal state Hamiltonian is given by

$$H_0 = \sum_{\mathbf{k}} \Psi_{\mathbf{k}}^\dagger (h_{\mathbf{k}} - \mu) \tau_z \Psi_{\mathbf{k}} \quad (1)$$

in the Nambu spinor basis  $\Psi_{\mathbf{k}} = (\psi_{\mathbf{k}}, \bar{\psi}_{\mathbf{k}})$ , where  $\psi_{\mathbf{k}}$  is a four-component Dirac spinor, and  $\bar{\psi}_{\mathbf{k}} = (-is_y)(\psi_{-\mathbf{k}}^\dagger)^T$  is its time-reversal hole partner. In the  $\mathbf{k} \cdot \mathbf{p}$  theory,  $h_{\mathbf{k}} = \sum_{i=x,y,z} v_i k_i \sigma_x s_i + m \sigma_z s_0$  with  $v_{x,y,z}$  being the velocities along three directions,  $m$  the Dirac mass, and  $\mathbf{s}$ ,  $\boldsymbol{\sigma}$  and  $\boldsymbol{\tau}$  the Pauli matrices acting on spin, orbital, and Nambu space, respectively [72, 73] (We set  $\hbar = 1$ ). Here  $\mu$  is the chemical potential which is assumed to be located in the conduction band. Furthermore, we consider

the intra-orbital ( $V_0 = V_z = V_{intra}$ ) and inter-orbital ( $V_x = V_y = V_{inter}$ ) long-ranged attractive (density-density) interaction between the Dirac fermions. By utilizing the Fierz identity [74–77], the density-density product of four-fermion interaction can be decomposed into the pairing terms

$$H_{int} = \sum_{\mathbf{k}, \mathbf{k}', i, j} \frac{V_i(\mathbf{k} - \mathbf{k}')}{8\Omega} \left[ \Psi_{\mathbf{k}}^\dagger \tau_+ M_{ij} \Psi_{\mathbf{k}} \right] \left[ \Psi_{\mathbf{k}'}^\dagger \tau_- M_{ij} \Psi_{\mathbf{k}'} \right] \quad (2)$$

where  $\Omega$  is the volume of the sample,  $M_{ij} \equiv \sigma_i s_j$  and  $\tau_{\pm} = \frac{1}{2}(\tau_x \pm i\tau_y)$ . The interaction potential  $V_i(\mathbf{k} - \mathbf{k}')$  can be decomposed by the Fermi-surface harmonics  $\varphi_\Gamma(\mathbf{k})$  for each irreducible representation of the crystal point group  $V_i(\mathbf{k} - \mathbf{k}') = \sum_\Gamma V_i^\Gamma \varphi_\Gamma(\mathbf{k}) [\varphi_\Gamma(\mathbf{k}')]^*$  [77, 78] where the sum over  $\Gamma$  contains all non-equivalent irreducible representations (IRs) of  $D_{2h}$  group [80]. The basis functions for each IR are clearly not unique, and have been truncated to the lowest order in momenta for simplicity. The calculation of the characteristic coefficients for interaction  $V_i^\Gamma$  can be found in Ref. [77]. The overall pairing functions are constructed by the orbital angular momentum part  $\varphi_\Gamma(\mathbf{k})$  and spin-orbital part  $M_{ij}$  listed in Table I. For the sake of simplicity, we only focus on the regime with the even  $s$ - and  $d$ -wave pairing function [ $\varphi_\Gamma(\mathbf{k}) = \varphi_\Gamma(-\mathbf{k})$ ] for the orbital part, which restricts ourselves to the remaining six antisymmetric pairing matrices  $M_{ij}$ , i.e.,  $[M_{ij}(-is_y)]^T = -M_{ij}(-is_y)$ , due to the Fermi-Dirac statistics. As a result of products of representations, the overall pairing function  $\varphi_\Gamma(\mathbf{k})M_{ij}$  and the orbital angular momentum part  $\varphi_\Gamma(\mathbf{k})$  may belong to different IRs.

In a weak-coupling regime, the Cooper pairs emerge mainly near the Fermi surface. Assuming that the Fermi level is located at the conduction bands, we can project out the conduction bands,  $\phi_{\mathbf{k}} = U_{\mathbf{k}}^\dagger \psi_{\mathbf{k}}$ , where  $U_{\mathbf{k}}$  is a  $4 \times 2$  matrix of conduction band eigenvectors such that the projection operator for the conduction band  $\mathcal{P}_c(\mathbf{k}) = U_{\mathbf{k}} U_{\mathbf{k}}^\dagger = \frac{1}{2}(1 + \frac{h_{\mathbf{k}}}{\epsilon_{\mathbf{k}}})$ . In this way,  $H_0$  is diagonalized and the pairing functions are transformed to  $N_{\mathbf{k}, \Gamma} = \varphi_{\Gamma'}(\mathbf{k}) U_{\mathbf{k}}^\dagger M_{ij} U_{\mathbf{k}}$  (see the fourth column in Table I). The superconducting pairing can be studied within the framework of the functional integral method [77, 81], and the corresponding partition function takes the form  $\mathcal{Z} = \int D[\Phi, \Phi^\dagger] e^{-\int_0^\beta d\tau \mathcal{L}[\Phi, \Phi^\dagger]}$  with the Lagrangian as  $\mathcal{L}[\Phi, \Phi^\dagger] = \frac{1}{2} \sum_{\mathbf{k}} \Phi_{\mathbf{k}, \tau}^\dagger \tau_0 \partial_\tau \Phi_{\mathbf{k}, \tau} + \tilde{H}_0(\tau) + \tilde{H}_{int}(\tau) - \mu \tilde{N}(\tau)$ , where  $\Phi_{\mathbf{k}} = (\phi_{\mathbf{k}}^\dagger \ \ \bar{\phi}_{\mathbf{k}}^\dagger)$  and  $\tilde{H}_0$ ,  $\tilde{H}_{int}$  and  $\tilde{N}$  are the projected Hamiltonian, the interaction term and the particle density operator respectively. The quartic interaction terms can be decoupled by performing the Hubbard-Stratonovich transformation meanwhile the superconductivity order parameters  $\eta_\Gamma$  are introduced. And the gap equations can be obtained by a variation of the action with respect to the order parameters.

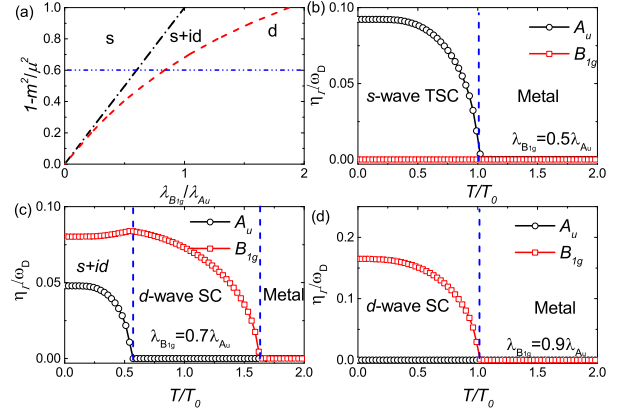


Figure 1. (a) Zero temperature phase diagram as a function of  $1 - m^2/\mu^2$  and  $\lambda_{B_{1g}}/\lambda_{A_u}$ . The temperature dependence order parameter  $\eta_{A_u}$  (b) for  $s$ -wave pairing (black lines with open circles),  $\eta_{B_{1g}}$  (d) for  $d$ -wave pairing (red lines with open squares), and (c) for  $s + id$ -wave pairing.  $\lambda_{A_u}$  is set to be  $1/2$  and  $1 - m^2/\mu^2 = 0.6$ . For regimes (b) and (d) with single order parameter, the temperature is in the unit of its transition temperature  $T_0 = T_c^\Gamma$ . For the mixed pairing regime (c),  $T_0 = T_c^{A_u}$ .

*Determination of the pairing symmetry* Now, we evaluate the transition temperature  $T_c^\Gamma$  for each pairing channel listed in Table I. It can be obtained by solving the linearized gap equation near the transition temperature  $T_c$  at which the order parameter is vanishingly small. Generally speaking,  $T_c^\Gamma \simeq 1.13\omega_D \exp\left[-\frac{1}{\lambda_\Gamma \langle N_{\mathbf{k}, \Gamma}^2 \rangle}\right]$  associated with each IR can be different. The transition temperature is dictated by two factors. The first one is the average of the square of the projected pairing matrices  $\langle N_{\mathbf{k}, \Gamma}^2 \rangle$  over the Fermi surface. The second one is the dimensionless coupling strength  $\lambda_\Gamma = 2g_\Gamma \rho(\mu)$  with the effective interaction  $g_\Gamma$  near the Fermi level and the density of states for the normal state  $\rho(\mu)$ . The inter-orbital interaction  $V_{i=x,y}(\mathbf{r} - \mathbf{r}')$  and the intra-orbital interaction  $V_{i=0,z}(\mathbf{r} - \mathbf{r}')$  give rise to pairing in the odd-parity channels ( $A_u, B_{1u}, B_{2u}, B_{3u}$ ) and even-parity channels ( $A_g, B_{1g}, B_{2g}, B_{3g}$ ), respectively. The four odd-parity pairing channels are generated from the local inter-orbital interaction and the transition temperatures satisfy  $T_c^{A_u} \gg T_c^{B_{1u}}, T_c^{B_{2u}}, T_c^{B_{3u}}$ . Thus we need only to consider the  $s$ -wave superconductivity belonging to the  $A_u$  representation among the four odd-parity pairing channels. In evaluating  $d$ -wave pairing matrices  $\langle N_{\mathbf{k}, B_{1g}}^2 \rangle$ ,  $\langle N_{\mathbf{k}, B_{2g}}^2 \rangle$ , and  $\langle N_{\mathbf{k}, B_{3g}}^2 \rangle$ , it is convenient to perform rescaling coordinate transformation  $\tilde{r}_i = \zeta_i r_i$  for  $i = x, y, z$  with the anisotropic factor  $\zeta_i = (v_x v_y v_z)^{1/3}/v_i$ , and we use  $\zeta_x = 1$ ,  $\zeta_y = 2$  and  $\zeta_z = 1/(\zeta_x \zeta_y) = 1/2$  throughout this work. Under the rescaling procedure, the Fermi surface average of the  $d$ -wave pairing matrices can be obtained analytically as  $\langle N_{\mathbf{k}, B_{1g}}^2 \rangle = \langle N_{\mathbf{k}, B_{2g}}^2 \rangle = \langle N_{\mathbf{k}, B_{3g}}^2 \rangle = 1$ . Without loss of generality, we assume

IRs	orbital	$\varphi_{\Gamma}(\mathbf{k})M_{ij}$	$N_{\mathbf{k},\Gamma}$	$\langle N_{\mathbf{k},\Gamma}^2 \rangle$
$A_g$	intra	$\varphi_0\sigma_0s_0$	$\varphi_0\tilde{\sigma}_0$	1
$B_{1g}$	intra	$\varphi_{xy}\sigma_0s_0$	$\varphi_{xy}\tilde{\sigma}_0$	1
$B_{2g}$	intra	$\varphi_{xz}\sigma_0s_0$	$\varphi_{xz}\tilde{\sigma}_0$	1
$B_{3g}$	intra	$\varphi_{yz}\sigma_0s_0$	$\varphi_{yz}\tilde{\sigma}_0$	1
$A_u$	inter	$\varphi_0\sigma_xs_0$	$\varphi_0\frac{\mathbf{p}\cdot\tilde{\sigma}}{\epsilon_{\mathbf{k}}}$	$1 - \frac{m^2}{\mu^2}$
$B_{1u}$	inter	$\varphi_0\sigma_ys_z$	$\varphi_0\frac{(\mathbf{p}\times\tilde{\sigma})_z}{\epsilon_{\mathbf{k}}}$	$\frac{2}{3}(1 - \frac{m^2}{\mu^2})$
$B_{2u}$	inter	$\varphi_0\sigma_ys_y$	$\varphi_0\frac{(\mathbf{p}\times\tilde{\sigma})_y}{\epsilon_{\mathbf{k}}}$	$\frac{2}{3}(1 - \frac{m^2}{\mu^2})$
$B_{3u}$	inter	$\varphi_0\sigma_ys_x$	$\varphi_0\frac{(\mathbf{p}\times\tilde{\sigma})_x}{\epsilon_{\mathbf{k}}}$	$\frac{2}{3}(1 - \frac{m^2}{\mu^2})$

Table I. Eight classes of the basis of the pairing functions according to  $D_{2h}$  point group symmetry. From left to right, each column shows the irreducible representations (IRs) of the point group  $D_{2h}$ , intra-orbital or inter-orbital pairing, the pairing channels  $\varphi_{\Gamma}(\mathbf{k})M_{ij}$  with antisymmetric matrices, the pairing functions  $N_{\mathbf{k},\Gamma}$  by projecting onto the states close to the Fermi surface, and the average over the Fermi surface  $\langle N_{\mathbf{k},\Gamma}^2 \rangle$  with  $\langle \dots \rangle$  stands for the Fermi surface average for arbitrary function  $\langle \dots \rangle = \sum_{\mathbf{k}} \dots \delta(\epsilon_{\mathbf{k}} - \mu) / \sum_{\mathbf{k}} \delta(\epsilon_{\mathbf{k}} - \mu)$  with  $\epsilon_{\mathbf{k}} = \sqrt{\sum_i v_i^2 k_i^2 + m^2}$ . The Pauli matrices  $\tilde{\sigma}_i$  denote the Kramers-degenerated conduction bands and we have introduced the notation  $\mathbf{p} = (v_x k_x, v_y k_y, v_z k_z)$ . The Fermi-surface harmonics  $\varphi_0 = 1$  and  $\varphi_{ij} = \frac{\sqrt{15}}{1 - m^2/\mu^2} \frac{v_i v_j k_i k_j}{\epsilon_{\mathbf{k}}^2}$  (for  $i, j = x, y, z$  and  $i \neq j$ ).

$g_{B_{1g}} > g_{B_{2g}} > g_{B_{3g}}$ . Under this condition, it is unlikely for the system to form the order parameter in  $B_{2g}$  and  $B_{3g}$  channels. Depending on the pairing interaction, we cannot avoid the possibility of the pairing belonging to the  $A_g$  representation. Since this order parameter breaks no additional symmetries besides the  $U(1)$  gauge symmetry, we disregard this conventional pairing for the further discussions. We have also checked numerically that the conclusion remains unchanged even with the inclusion of this pairing.

From now on, we focus on the topological nontrivial phases with  $s$ - and  $d$ -wave pairing which belong to two different irreducible representations  $A_u$  and  $B_{1g}$ , respectively. Generally,  $\eta_{\Gamma}$  are complex which can be parameterized as  $\eta_{\Gamma} = |\eta_{\Gamma}|e^{i\phi_{\Gamma}}$  where  $|\eta_{\Gamma}|$  and  $\phi_{\Gamma}$  are real. We consider the case that the phase difference for  $s$ -wave and  $d$ -wave pairing  $\Delta\phi = \phi_{A_u} - \phi_{B_{1g}}$ , and the order parameter for  $s$ -wave pairing is real, i.e.  $\phi_{A_u} = 0$ . By minimizing the free energy with the two superconducting order parameters, the relative phase should be  $\Delta\phi = \pm\pi/2$  if they coexist [77]. Then the pairing function can be expressed as  $\sum_{\Gamma} \eta_{\Gamma} N_{\mathbf{k}}^{\Gamma} = \eta_{A_u} N_{\mathbf{k},A_u} - i\eta_{B_{1g}} N_{\mathbf{k},B_{1g}}$ , with  $N_{\mathbf{k},A_u} = \varphi_0 \frac{\mathbf{p}\cdot\tilde{\sigma}}{\epsilon_{\mathbf{k}}}$  and  $N_{\mathbf{k},B_{1g}} = \varphi_{xy}\tilde{\sigma}_0$ . Thus, the projected Bogoliubov-de Gennes (BdG) Hamiltonian can be

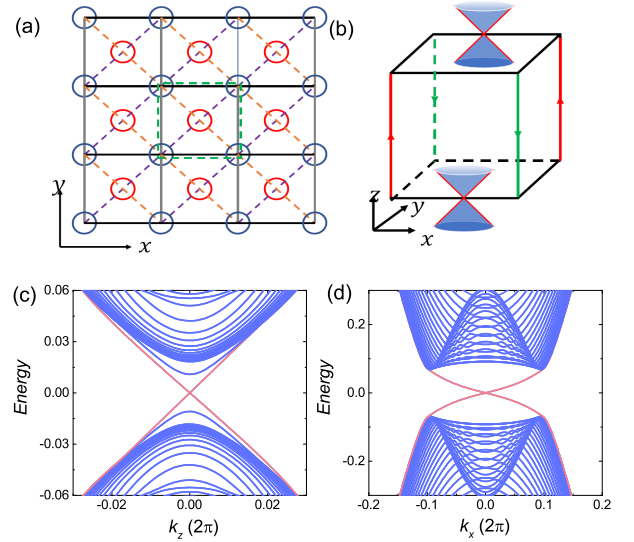


Figure 2. (a) Schematic of cross section lattice and the boundary of the x-y plane. The unit cell (the dash green box) consists of two sublattices indicated by blue and red circles. (b) The schematic of Majorana hinge modes and gapless Majorana surface modes in the case of  $s + id$ -wave pairing. (c) The dispersion spectrum of Majorana hinge modes for quasi-1D hinges along  $z$  direction with  $L_x = L_y = 60$ . (d) The dispersion spectrum of the Majorana surface modes in the x-y plane. The open boundary condition is adopted along  $z$  direction with the height  $L_z = 200$  and the periodic boundaries are adopted along  $x$  and  $y$  directions (see Sec. VII of Ref. [77]). The chemical potential  $\mu = 0.5$ .

expressed as,

$$\tilde{h}_{\mathbf{k}}^{BdG} = (\epsilon_{\mathbf{k}} - \mu)\tilde{\sigma}_0\tau_z + \frac{\eta_{A_u}}{\mu}\mathbf{p}\cdot\tilde{\sigma}\tau_x + \frac{\sqrt{15}\eta_{B_{1g}}v_xv_yk_xk_y}{\mu^2 - m^2}\tilde{\sigma}_0\tau_y. \quad (3)$$

The gap equations are reduced to a pair of coupled self-consistent equations of superconducting gap for the two pairing amplitudes  $\eta_{A_u}(T)$  and  $\eta_{B_{1g}}(T)$ .

*s + id wave pairing state* Now we turn to explore the possibility of a mixed  $s + id$ -wave pairing which breaks the time-reversal symmetry spontaneously. Figure 1(a) shows the phase diagram at zero temperature as function of  $1 - m^2/\mu^2$  and the interaction ratio  $\lambda_{B_{1g}}/\lambda_{A_u}$  with fixed  $\lambda_{A_u}$  to illustrate the competition between the  $s$ - and  $d$ -wave pairing superconductivity. The red and black dotted lines indicate the phase boundary separating the purely  $s$  ( $\eta_{A_u}(0) \neq 0, \eta_{B_{1g}}(0) = 0$ ) or  $d$ -wave pairing ( $\eta_{A_u}(0) = 0, \eta_{B_{1g}}(0) \neq 0$ ) and the mixed  $s + id$ -wave pairing ( $\eta_{A_u}(0), \eta_{B_{1g}}(0) \neq 0$ ). The competition between the  $s$ - and  $d$ -wave pairing channels can lead to either purely  $s$ - or  $d$ -wave pairing state, or a mixed  $s + id$ -wave state. It is intuitively clear that for such an  $s + id$ -solution to be held, pairing strengths  $\lambda_{A_u}$  and  $\lambda_{B_{1g}}$  need to be comparable: otherwise, a  $s$ -wave or a  $d$ -wave will dominate. Adjusting the chemical potential toward the band edge, the region for the mixed pairing shrinks. Thus, the mixed

pairing is more likely to occur in a system when the chemical potential locates away from the band edge.

Then we discuss the behaviors of two different order parameters  $\eta_{A_u}$  and  $\eta_{B_{1g}}$  at finite temperature, which are calculated by solving the gap equations as a function of temperature for several values of  $\lambda_{B_{1g}}/\lambda_{A_u}$  and fixed  $1 - m^2/\mu^2 = 0.6$ . As shown in Fig. 1(b)(d), if  $\lambda_{B_{1g}}/\lambda_{A_u} < r_{max} = [(1 - m^2/\mu^2)^{-1} - \frac{14}{15}\lambda_{A_u}]^{-1}$  or  $\lambda_{B_{1g}}/\lambda_{A_u} > r_{min} = 1 - m^2/\mu^2$  [77], it is a pure  $s$  or  $d$ -wave superconductivity whose critical temperature is precisely determined by  $T_c^F$ , that the superconducting transition is only specific to one of the IRs. The mixed paired state appears at the intermediate region  $\lambda_{B_{1g}}/\lambda_{A_u} \in (r_{min}, r_{max})$ . As shown in Fig. 1(c), for  $\lambda_{B_{1g}}/\lambda_{A_u} = 0.7$  ( $\in (r_{min}, r_{max})$ ), as the temperature decreases down to a certain value  $\sim 1.63T_0$ ,  $\eta_{B_{1g}}$  first appears. After then, the  $s$  wave pairing  $\eta_{A_u}$  appears and  $\eta_{B_{1g}}$  increases gradually with temperature until  $\sim 0.55T_0$ . After that, the  $d$ -wave component reduces while the  $s$ -wave component grows up as temperature decreases to zero. This indicates that, with decreasing the temperature, it undergoes a topological phase transition from pure  $d$ -wave superconductivity to  $s + id$ -wave superconductivity in specific conditions.

*Majorana hinge and surface modes in the  $s + id$  wave pairing state* The  $s + id$ -wave pairing superconducting state is higher-order topologically nontrivial, which is revealed from the existence of Majorana hinge and surface modes. We adopt the tight-binding approximation on a cubic lattice with the lattice orientation of the x-y plane as shown in Fig. 2(a)[77]. Four chiral Majorana hinge modes and two Majorana surface modes are illustrated in Fig. 2(b). The origin of the topological hinge modes in  $s + id$ -wave pairing state can be heuristically explained in the following picture. According to the odd-parity superconductivity criterion [70], the system of the single  $s$ -wave pairing ( $A_u$ ) should be a time-reversal invariant topological superconductor with massless helical Majorana modes on the surface. The inclusion of the  $d$ -wave order parameter gaps out the Dirac cones of the Majorana surface modes on the surfaces parallel to the z-axis as its relative  $\pi/2$  phase to the  $s$ -wave order parameter breaks the time reversal symmetry. However, the  $d$ -wave pairing gap function vanishes at the mirror planes and acts as mass domain walls for Majorana surface modes. Consequently, the chiral Majorana hinge modes are formed around the domain wall or along the hinges. The dispersion spectra for the Majorana hinge states as a function of  $k_z$  are presented in Fig. 2(c). The gapless Majorana hinge modes in the gap are marked by the red lines and localized near the four hinges along the z-direction. Their dispersions are linear in  $k_z$ ,  $E_{hinge} = \pm \frac{\eta_{A_u}}{\mu} v_z k_z$ , obtained from the projected BdG Hamiltonian in Eq. (3). On the top and bottom surface of the x-y plane, the  $d$ -wave pairing breaks the time-reversal symmetry, but does not open the band gap of surface Majorana states. The

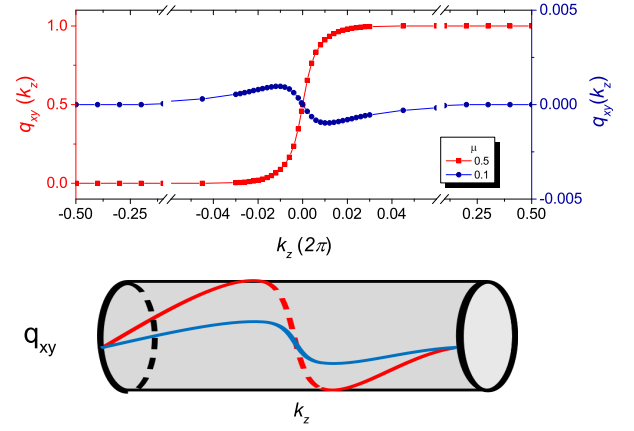


Figure 3. The quadrupole moment  $q_{xy}(k_z)$  as a function of  $k_z$  for  $\mu = 0.5$  (red) with the winding number  $\Delta q_{xy} = 1$  and 0.1 (blue) with  $\Delta q_{xy} = 0$ . The bottom:  $q_{xy}$  is rolled as a tube with  $q_{xy}$  module 1. The other parameters used are the same as Fig. 2.

dispersion spectra are plotted in Fig. 2(d), in which the gapless Majorana surface states are marked by the red lines. The BdG Hamiltonian with the odd-parity  $s$ -wave pairing ( $\propto \sigma_x \tau_x$ ) possesses the time-reversal symmetry  $\mathcal{T} = is_y \mathcal{K}$  and the inversion symmetry  $\tilde{\mathcal{I}} \equiv \mathcal{I} \tau_z = \sigma_z \tau_z$ . The inclusion of the  $d$ -wave pairing ( $\propto k_x k_y \tau_y$ ) breaks either  $\mathcal{T}$  or  $\tilde{\mathcal{I}}$ , but preserves  $\tilde{\mathcal{I}} \mathcal{T}$ . This combined symmetry makes the Majorana hinge modes at diagonal hinges and the Majorana surface states at the opposite surface related by the symmetry operation  $\tilde{\mathcal{I}} \mathcal{T}$ .

*Topological invariants* Now we come to discuss the topological invariant which is related to the Majorana hinge modes. We take the periodic condition along the z axis such that  $k_z$  is a good quantum number. The quadrupole moment for each  $k_z$  is given by [82–84]

$$q_{xy}(k_z) = \frac{1}{2\pi} \text{Im} \log \left[ \text{Det}[U_{k_z}^\dagger Q U_{k_z}] \sqrt{\text{Det} Q^\dagger} \right], \quad (4)$$

where the matrix  $U_{k_z}$  is constructed by the occupied ground states,  $Q = e^{2\pi i \hat{x} \hat{y} / L_x L_y}$ ,  $\hat{x}$  and  $\hat{y}$  are the position operators, and  $L_x$  and  $L_y$  the length of our system in x and y direction, respectively. Generally the particle-hole symmetry  $\mathcal{P}$  is broken for a specific  $k_z$  as the two states at  $k_z$  and  $-k_z$  are connected by the  $\mathcal{P}$  symmetry. However the symmetry restores at  $k_z = 0$  and  $\pi$  (half of the reciprocal lattice vector), i.e., the particle-hole invariant momentum. At these momenta, we can prove that the quadrupole moment  $q_{xy}$  is quantized to be 0 or 1/2 module 1 [77]. Quantized quadrupole moment of  $q_{xy} = 1/2$  means the existence of the corner states of zero energy, a signature of the second-order topological phase [30, 31]. The quantization is removed once  $k_z$  moves away the invariant momentum. Additions of the corner states for different  $k_z$  evolve into the chiral hinge states in three dimensions. Furthermore, the  $\mathcal{P}$  symmetry con-

nects the unoccupied states at momentum  $k_z$  with unoccupied states at  $-k_z$ , which gives  $q_{xy}(k_z) + q_{xy}(-k_z) = 0$  for a trivial case and 1 for a nontrivial case. Thus in the  $s + id$ -wave pairing state, a winding number can be introduced  $\Delta q_{xy} = \int_{-\pi}^{\pi} dk_z \partial_{k_z} q_{xy}(k_z)$ . Two  $k_z$ -dependent quadrupole moments for trivial (blue line with circle) and nontrivial (red line with square) cases are plotted in Fig. 3. For  $\mu = 0.5$ , it is found that  $q_{xy} = 1/2$  at  $k_z = 0$ , and 0 at  $k_z = \pi$ . The winding number  $\Delta q_{xy} = 1$ , which means the state is topologically nontrivial and is related to the presence of chiral Majorana hinge modes. In this way, we establish a bulk-hinge correspondence in the topologically nontrivial superconducting state.

This work was supported by the Ministry of Science and Technology of China under Grant No. 2019YFA0308603, Natural Science Foundation of China under Grant No. 11774317, and Natural Science Foundation of Zhejiang under Grant No. LQ20A040003.

---

\* sshen@hku.hk

- [1] A. Yu Kitaev, Fault-tolerant quantum computation by anyons, *Ann. Phys. (Amsterdam)* 303, 2 (2003).
- [2] C. Nayak, S. H. Simon, A. Stern, M. Freedman, and S. Das Sarma, Non-Abelian anyons and topological quantum computation, *Rev. Mod. Phys.* 80, 1083 (2008).
- [3] F. Wilczek, Majorana returns, *Nat. Phys.* 5, 614(2009).
- [4] J. Alicea, New directions in the pursuit of Majorana fermions in solid state systems, *Rep. Prog. Phys.* 75, 076501 (2012).
- [5] C. W. J Beenakker, Search for Majorana fermions in superconductors, *Annu. Rev. Condens. Matter Phys.* 4, 113 (2013).
- [6] S. R. Elliott and M. Franz, Colloquium: Majorana fermions in nuclear, particle, and solid-state physics, *Rev. Mod. Phys.* 87, 137(2015).
- [7] V. Mourik, K. Zuo, S. M. Frolov, S. R. Plissard, E. P. A. M. Bakkers, and L. P. Kouwenhoven, Signatures of Majorana fermions in hybrid superconductor-semiconductor nanowire devices, *Science* 336, 1003 (2012).
- [8] A. Das, Y. Ronen, Y. Most, Y. Oreg, M. Heiblum, and H. Shtrikman, Zero-bias peaks and splitting in an Al-InAs nanowire topological superconductor as a signature of Majorana fermions, *Nat. Phys.* 8, 887 (2012).
- [9] L. P. Rokhinson, X. Liu, and J. K. Furdyna, The fractional a.c. Josephson effect in a semiconductor-superconductor nanowire as a signature of Majorana particles, *Nat. Phys.* 8, 795 (2012).
- [10] S. Nadj-Perge, I. K. Drozdov, J. Li, H. Chen, S. Jeon, J. Seo, A. H. MacDonald, B. A. Bernevig, and A. Yazdani, Observation of Majorana fermions in ferromagnetic atomic chains on a superconductor, *Science* 346, 602 (2014).
- [11] H. Zhang et al., Quantized Majorana conductance, *Nature (London)* 556, 74 (2018).
- [12] H.-H. Sun, K.-W. Zhang, L.-H. Hu, C. Li, G.-Y. Wang, H.-Y. Ma, Z.-A. Xu, C.-L. Gao, D.-D. Guan, Y.-Y. Li, C. Liu, D. Qian, Y. Zhou, L. Fu, S.-C. Li, F.-C. Zhang, and J.-F. Jia, Majorana zero mode detected with spin selective Andreev reflection in the vortex of a topological superconductor, *Phys. Rev. Lett.* 116, 257003 (2016).
- [13] D. Wang, L. Kong, P. Fan, H. Chen, S. Zhu, W. Liu, L. Cao, Y. Sun, S. Du, J. Schneeloch et al., Evidence for Majorana bound states in an iron-based superconductor, *Science* 362, 333 (2018).
- [14] R. M. Lutchyn, E. P. A. M. Bakkers, L. P. Kouwenhoven, P. Krogstrup, C. M. Marcus, and Y. Oreg, Majorana zero modes in superconductor-semiconductor heterostructures, *Nat. Rev. Mater.* 3, 52 (2018).
- [15] G. E. Volovik, Fermion zero modes on vortices in chiral superconductors, *J. Exp. Theor. Phys. Lett.* 70, 609 (1999).
- [16] N. Read and D. Green, Paired states of fermions in two dimensions with breaking of parity and time-reversal symmetries and the fractional quantum Hall effect, *Phys. Rev. B* 61, 10267 (2000).
- [17] D. A. Ivanov, Non-Abelian statistics of half-quantum vortices in p-wave superconductors, *Phys. Rev. Lett.* 86, 268 (2001).
- [18] A. Yu Kitaev, Unpaired Majorana fermions in quantum wires, *Phys. Usp.* 44, 131 (2001).
- [19] X.-L. Qi, T. L. Hughes, and S.-C. Zhang, Chiral topological superconductor from the quantum Hall state, *Phys. Rev. B* 82, 184516 (2010).
- [20] S. B. Chung, X.-L. Qi, J. Maciejko, and S.-C. Zhang, Conductance and noise signatures of Majorana backscattering, *Phys. Rev. B* 83, 100512 (2011).
- [21] J. Wang, Q. Zhou, B. Lian, and S.-C. Zhang, Chiral topological superconductor and half-integer conductance plateau from quantum anomalous Hall plateau transition, *Phys. Rev. B* 92, 064520 (2015).
- [22] Q. L. He, L. Pan, A. L. Stern, E. Burks, X. Che, G. Yin, J. Wang, B. Lian, Q. Zhou, E. S. Choi, K. Murata, X. Kou, T. Nie, Q. Shao, Y. Fan, S.-C. Zhang, K. Liu, J. Xia, and K. L. Wang, Chiral Majorana fermion modes in a quantum anomalous Hall insulator-superconductor structure, *Science* 357, 294 (2017).
- [23] W. Ji and X.-G. Wen,  $1/2(e^2/h)$  Conductance plateau without 1D chiral Majorana fermions, *Phys. Rev. Lett.* 120, 107002 (2018).
- [24] Y. Huang, F. Setiawan, and J. D. Sau, Disorder-induced half-integer quantized conductance plateau in quantum anomalous Hall insulator-superconductor structures, *Phys. Rev. B* 97, 100501 (2018).
- [25] B. Lian, J. Wang, X.-Q. Sun, A. Vaezi, and S.-C. Zhang, Quantum phase transition of chiral Majorana fermions in the presence of disorder, *Phys. Rev. B* 97, 125408 (2018).
- [26] M. Kayyalha, D. Xiao, R. Zhang, J. Shin, J. Jiang, F. Wang, Y.-F. Zhao, R. Xiao, L. Zhang, K. M. Fijalkowski, P. Mandal, M. Winnerlein, C. Gould, Q. Li, L. W. Molenkamp, M. H. W. Chan, N. Samarth, and C.-Z. Chang, Absence of evidence for chiral Majorana modes in quantum anomalous Hall-superconductor devices, *Science* 367, 64 (2020).
- [27] G. Struelli, W. Belzig, M.-S. Choi, and C. Bruder, Interferometric and noise signatures of Majorana fermion edge states in transport experiments, *Phys. Rev. Lett.* 107, 136403 (2011).
- [28] B. Lian, X.-Q. Sun, A. Vaezi, X.-L. Qi, and S.-C. Zhang, Topological quantum computation based on chiral Majorana fermions, *Proc. Natl. Acad. Sci. U.S.A.* 115, 10938 (2018).

- [29] C. A. Li, J. Li, S.-Q. Shen, Majorana-Josephson interferometer, *Phys. Rev. B*, 99, 100504(R) (2019).
- [30] W. A. Benalcazar, B. Andrei Bernevig, and T. L. Hughes, Quantized electric multipole insulators, *Science* 357, 61 (2017).
- [31] W. A. Benalcazar, B. Andrei Bernevig, and T. L. Hughes, Electric multipole moments, topological multipole moment pumping, and chiral hinge states in crystalline insulators, *Phys. Rev. B* 96, 245115 (2017).
- [32] F. Schindler, A. M. Cook, M. G. Vergniory, Z. Wang, S. S. P. Parkin, B. Andrei Bernevig, and T. Neupert, Higher-order topological insulators, *Sci. Adv.* 4, eaat0346 (2018).
- [33] X. Zhu, Second-order topological superconductors with mixed pairing, *Phys. Rev. Lett.* 122, 236401 (2019).
- [34] J. Langbehn, Y. Peng, L. Trifunovic, F. von Oppen, and P. W. Brouwer, Reflection-symmetric second-order topological insulators and superconductors, *Phys. Rev. Lett.* 119, 246401 (2017).
- [35] M. Ezawa, Higher-order topological insulators and semimetals on the breathing kagome and pyrochlore lattices, *Phys. Rev. Lett.* 120, 026801 (2018).
- [36] E. Khalaf, Higher-order topological insulators and superconductors protected by inversion symmetry, *Phys. Rev. B* 97, 205136 (2018).
- [37] S. Franca, J. van den Brink, and I. C. Fulga, An anomalous higher-order topological insulator, *Phys. Rev. B* 98, 201114(R) (2018).
- [38] D. Călugăru, V. Juričić, and B. Roy, Higher-order topological phases: A general principle of construction, *Phys. Rev. B* 99, 041301(R) (2019).
- [39] C. A. Li and S. S. Wu, Topological states in generalized electric quadrupole insulators, *Phys. Rev. B* 101, 195309 (2020).
- [40] F. Schindler, Z. Wang, M. G. Vergniory, A. M. Cook, A. Murani, S. Sengupta, A. Yu Kasumov, R. Deblock, S. Jeon, I. Drozdov, H. Bouchiat, S. Guéron, A. Yazdani, B. A. Bernevig, and T. Neupert, Higher-order topology in bismuth, *Nat. Phys.* 14, 918 (2018).
- [41] S. Imhof, C. Berger, F. Bayer, J. Brehm, L. W. Molenkamp, T. Kiessling, F. Schindler, C. Hua Lee, M. Greiter, T. Neupert, and R. Thomale, Topological-circuit realization of topological corner modes, *Nat. Phys.* 14, 925 (2018).
- [42] M. Serra-Garcia, V. Peri, R. Süssstrunk, O. R. Bilal, T. Larsen, L. G. Villanueva, and S. D. Huber, Observation of a phononic quadrupole topological insulator, *Nature (London)* 555, 342 (2018).
- [43] C. W. Peterson, W. A. Benalcazar, T. L. Hughes, and G. Bahl, A quantized microwave quadrupole insulator with topologically protected corner states, *Nature (London)* 555, 346 (2018).
- [44] X. Zhang, H.-X. Wang, Z.-K. Lin, Y. Tian, B. Xie, M.-H. Lu, Y.-F. Chen, and J.-H. Jiang, Second-order topology and multidimensional topological transitions in sonic crystals, *Nat. Phys.* 15, 582 (2019).
- [45] J. Niu, T. Yan, Y. Zhou, Z. Tao, X. Li, W. Liu, L. Zhang, S. Liu, Z. Yan, Y. Chen et al., Simulation of higher-order topological phases and related topological phase transitions in a superconducting qubit, arXiv:2001.03933.
- [46] Z. Yan, F. Song, and Z. Wang, Majorana Kramers pairs in a high-temperature platform, *Phys. Rev. Lett.* 121, 096803 (2018).
- [47] Y. Wang, M. Lin, and T. L. Hughes, Weak-pairing higher order topological superconductors, *Phys. Rev. B* 98, 165144 (2018).
- [48] Q. Wang, C.-C. Liu, Y.-M. Lu, and F. Zhang, High temperature Majorana corner states, *Phys. Rev. Lett.* 121, 186801 (2018).
- [49] Z. Wu, Z. Yan, and W. Huang, Higher-order topological superconductivity: possible realization in Fermi gases and  $\text{Sr}_2\text{RuO}_4$ , *Phys. Rev. B* 99, 020508(R) (2019).
- [50] C.-H. Hsu, P. Stano, J. Klinovaja, and D. Loss, Majorana Kramers pairs in higher-order topological insulators, *Phys. Rev. Lett.* 121, 196801 (2018).
- [51] T. Liu, J. J. He, and F. Nori, Majorana corner states in a two-dimensional magnetic topological insulator on a high-temperature superconductor, *Phys. Rev. B* 98, 245413 (2018).
- [52] Y. Volpez, D. Loss, and J. Klinovaja, Second-order topological superconductivity in  $\pi$ -junction Rashba layers, *Phys. Rev. Lett.* 122, 126402 (2019).
- [53] R.-X. Zhang, W. S. Cole, and S. Das Sarma, Helical hinge Majorana modes in iron-based superconductors, *Phys. Rev. Lett.* 122, 187001 (2019).
- [54] C. Zeng, T. D. Stanescu, C. Zhang, V. W. Scarola, and S. Tewari, Majorana corner modes with solitons in an attractive Hubbard-Hofstadter model of cold atom optical lattices, *Phys. Rev. Lett.* 123, 060402 (2019).
- [55] Z. Yan, Higher-order topological odd-parity superconductors, *Phys. Rev. Lett.* 123, 177001 (2019).
- [56] S.-B. Zhang and B. Trauzettel, Detection of second-order topological superconductors by Josephson junctions, *Phys. Rev. Research* 2, 012018 (2020).
- [57] X.-H. Pan, K.-J. Yang, L. Chen, G. Xu, C.-X. Liu, and X. Liu, Lattice-symmetry-assisted second-order topological superconductors and Majorana patterns, *Phys. Rev. Lett.* 123, 156801 (2019).
- [58] S. Franca, D. V. Efremov, and I. C. Fulga, Phase-tunable second-order topological superconductor, *Phys. Rev. B* 100, 075415 (2019).
- [59] R.-X. Zhang, W. S. Cole, X. Wu, and S. Das Sarma, Higher-order topology and nodal topological superconductivity in Fe(Se,Te) heterostructures, *Phys. Rev. Lett.* 123, 167001 (2019).
- [60] J. Ahn and B.-J. Yang, Higher-order topological superconductivity of spin-polarized fermions, *Phys. Rev. Research* 2, 012060 (2020).
- [61] M. Kheirkhah, Y. Nagai, C. Chen, and F. Marsiglio, Majorana corner flat bands in two-dimensional second order topological superconductors, *Phys. Rev. B* 101, 104502 (2020).
- [62] S. Ali Akbar Ghorashi, T. L. Hughes, and E. Rossi, Vortex and surface phase transitions in superconducting higher order topological insulators, *Phys. Rev. Lett.* 125, 037001 (2020).
- [63] Y.-T. Hsu, W. S. Cole, R.-X. Zhang, and J. D. Sau, Inversion-protected higher order topological superconductivity in monolayer  $\text{WTe}_2$ , *Phys. Rev. Lett.* 125, 097001 (2020).
- [64] B. Roy, Higher-order topological superconductors in  $\mathcal{P}$ -,  $\mathcal{T}$ -odd quadrupolar Dirac materials, *Phys. Rev. B* 101, 220506(R) (2020).
- [65] Song-Bo Zhang, Alessio Calzona, and Björn Trauzettel, All-electrically tunable networks of Majorana bound states, *Phys. Rev. B* 102, 100503(R) (2020).

- [66] B. Jäck, Y. L. Xie, J. Li, S. Jeon, B. A. Bernevig, and A. Yazdani, Observation of a Majorana zero mode in a topologically protected edge channel, *Science* 364, 1255 (2019).
- [67] Y. Peng and Y. Xu, Proximity-induced Majorana hinge modes in antiferromagnetic topological insulators, *Phys. Rev. B* 99, 195431 (2019).
- [68] Y.-J. Wu, J. Hou, X. Luo, Y. Li, and C. Zhang, In-plane Zeeman field induced Majorana corner and hinge modes in an s-wave superconductor heterostructure, *Phys. Rev. Lett.* 124, 227001 (2020).
- [69] C. M. Yue, Y. F. Xu, Z. D. Song, H. M. Weng, Y. M. Lu, C. Fang, and X. Dai, Symmetry-enforced chiral hinge states and surface quantum anomalous Hall effect in the magnetic axion insulator  $\text{Bi}_{2-x}\text{Sm}_x\text{Se}_3$ , *Nat. Phys.* 15, 577 (2019).
- [70] L. Fu and E. Berg, Odd-parity topological superconductors: theory and application to  $\text{Cu}_x\text{Bi}_2\text{Se}_3$ , *Phys. Rev. Lett.* 105, 097001 (2010).
- [71] M. Sato, Topological odd-parity superconductors, *Phys. Rev. B* 81, 220504(R) (2010).
- [72] S. Q. Shen, *Topological insulators: Dirac equation in condensed matter*, 2nd ed. (Springer, Singapore, 2017).
- [73] S. Q. Shen, W. Y. Shan and H. Z. Lu, Topological insulator and the Dirac equation, *Spin* 01, 33 (2011).
- [74] O. Vafek, Interacting fermions on the honeycomb bilayer: From weak to strong coupling, *Phys. Rev. B* 82, 205106 (2010).
- [75] L. Savary, J. Ruhman, J. W. F. Venderbos, L. Fu, and P. A. Lee, Superconductivity in three-dimensional spin-orbit coupled semimetals, *Phys. Rev. B* 96, 214514 (2017).
- [76] J. W. F. Venderbos, L. Savary, J. Ruhman, P. A. Lee, and L. Fu, Pairing states of spin-3/2 fermions: symmetry-enforced topological gap functions, *Phys. Rev. X* 8, 011029 (2018).
- [77] See Supplemental Material at [URL to be added by publisher] for details of (Sec. SI) Symmetry of BdG Hamiltonian, (Sec. SII) Expansion of the interaction potential in Fermi-surface Harmonics, (Sec. SIII) Derivation of the Ginzburg-Landau free energy, (Sec. SIV) The multi-components basis functions in each representation, (Sec. SV) Spontaneous time reversal symmetry breaking for the mixed  $s$  and  $d$  wave pairing state, (Sec, SVI) Zero temperature phase boundary for mixed  $s + id$  wave pairing state, (Sec. SVII) Tight-binding model, and (Sec. SVIII) The topological invariant for  $s + id$  wave pairing state, which includes Refs. [74, 75, 78–84]
- [78] T. Nomoto, K. Hattori, and H. Ikeda, Classification of multipole superconductivity in multiorbital systems and its implications, *Phys. Rev. B* 94, 174513 (2016).
- [79] P. B. Allen, Fermi-surface harmonics: A general method for nonspherical problems. Application to Boltzmann and Klichberg equations, *Phys. Rev. B* 13, 1416 (1976).
- [80] M. Dresselhaus, *Applications of group theory to the physics of solids* (MIT, Cambridge, MA, 2002).
- [81] A. Altland and B. Simons, *Condensed matter field theory* (Cambridge University Press, 2010).
- [82] C. A. Li, B. Fu, Z. A. Hu, J. Li and S. Q. Shen, Topological phase transitions in disordered electric quadrupole Insulators, *Phys. Rev. Lett.* 125, 166801 (2020).
- [83] B. Kang, K. Shiozaki, and G. Y. Cho, Many-body order parameters for multipoles in solids, *Phys. Rev. B* 100, 245134 (2019).
- [84] W. A. Wheeler, L. K. Wagner, and T. L. Hughes, Many-body electric multipole operators in extended systems, *Phys. Rev. B* 100, 245135 (2019).